Hindawi
Advances in Materials Science and Engineering
Volume 2022, Article ID 7480361, 12 pages
https://doi.org/10.1155/2022/7480361

Research Article

The Permeability Alternation of Shale Fractures due to Sc-CO_2 Soaking: Implications for Sc-CO_2 Fracturing and Deep CO_2 Sequestration in Shale Reservoirs

Zhaohui Lu,[1] Yunzhong Jia,[1] Jiankun Zhou,[1] Pei He,[1] Menglai Li,[1] Zhengyang Song,[2] and Xin Cai[3]

[1]*National and Local Joint Engineering Research Center of Shale Gas Exploration and Development, Chongqing Institute of Geology and Mineral Resources, Chongqing 401120, China*
[2]*Department of Civil Engineering, School of Civil & Resource Engineering, University of Science & Technology Beijing, Beijing 100083, China*
[3]*School of Resources and Safety Engineering, Central South University, Changsha, Hunan 410083, China*

Correspondence should be addressed to Yunzhong Jia; yunzhong.jia@geo.uu.se

Received 18 August 2021; Revised 5 January 2022; Accepted 6 January 2022; Published 21 January 2022

Academic Editor: Antonio Riveiro

The shale fracture permeability is critical in determining gas production and deep CO_2 sequestration performance. Moreover, how shale fracture permeability evolves after interactions with supercritical carbon dioxide (Sc-CO_2) should be understood to constrain the shale reservoir permeability and evaluate the long-term sealing ability of shale formations. In this research, we conducted soaking experiments with shale fractures and Sc-CO_2 at various times and then measured the shale fracture permeability and hydraulic aperture evolution under different stress states. Additionally, we quantify the chemical compositions, pore characteristics, fracture surface roughness alternation through X-ray diffraction, nuclear magnetic resonance, scanning electron microscope, and optical profilometry techniques. Our results indicate that soaking with Sc-CO_2 will dramatically increase the shale fracture permeability and aperture due to the calcite and dolomite dissolution. This free-face dissolution process will remove the mineral particles in the fracture surface, resulting in larger pores, peaks, and valleys in the fracture surfaces. This process may last for seven days, and after that, chemical reactions may terminate, and the rock-Sc-CO_2 system turns stable. Our results explain how Sc-CO_2 alters the shale fracture permeability through the chemical dissolution of specific minerals from a microscale analysis.

1. Introduction

Shale gas production has boomed during the last decades due to the technological advancements in horizontal drilling and multistage fracturing in Sichuan Basin, China [1–3]. As the primary technology during shale gas development, hydraulic fracturing is implemented by injecting a large amount of water and sand proppants [4–6]. Researches indicated that potential drawbacks include massive consumption of water, underground water contamination, and possible fluid injection-induced seismic events [7–10]. Moreover, the high clay content in shale formation and its chemical reaction with water will induce the swelling phenomenon and induce the permeability enhancement performance not to be satisfied [11]. Thus, some other fracturing fluids have been proposed to replace conventional water-based fracturing fluids, such as nitrogen and supercritical carbon dioxide (Sc-CO_2) [12, 13]. Sc-CO_2 may be a good choice due to its characteristics of high density and low viscosity under the reservoir conditions, in which the temperature is higher than 31.1°C and the pressure is higher than 7.38 MPa [14]. Recent research also validated that the Sc-CO_2 may decrease the shale reservoir breakdown pressure and create complex fracture networks due to its low viscosity property, benefiting shale reservoirs permeability enhancement [15–19].

After the Sc-CO_2 injection into the shale formation, the shale rock properties may change due to the stress (mechanical) and chemical reactions. The research on the interactions between shale rock and Sc-CO_2 is also a hot topic in the oil and gas industry. The experimental results show that the adsorption of Sc-CO_2 induces the shale matrix swelling, which alters the mechanical properties of shale [20–22]. Moreover, experimental results found that the interactions between shale rock and Sc-CO_2 would significantly decrease the mechanical properties of shale rock, including uniaxial compressive strength (UCS), tensile strength, and elastic modulus [23–26]. Scholars commonly explain this weakening effect from the aspects of microscale structural alternation [27–29]. Experimental results found that the shale's specific surface area and porosity will increase after the treatment by Sc-CO_2 through dissolving the organic matter in the shale [30]. Nuclear magnetic resonance (NMR) measurements with shale from Gippsland Basin, Australia, indicate the pore volume will increase after exposure to Sc-CO_2, which results from chemical reactions, including dissolution and precipitation of kaolinite, natrojarosite, silica, and gypsum [31]. Alemu et al. found that the carbonate-rich shale will react with plagioclase and clay minerals, which induce the CO_2 sequestration in the shale as the calcite [32]. In situ experiments in Utica shale indicate that CO_2 will interact with Kergon and illite-smectite clays in shale, which means that those shale plays have higher CO_2 storage capacity [33]. Experiments with Eagle Ford and Mancos shales indicate that quartz content increases after the treatment with Sc-CO_2, while clay and carbonate minerals' contents decrease. Thus, the mineral carbonation trapping could be an effective mechanism for long-term CO_2 storage in shale reservoirs [34]. As mentioned above, researchers attempted to analyse the interaction between Sc-CO_2 and various kinds of shale from the mechanical aspects. As the main fluid channels for shale gas during the production, fracture permeability plays a vital role in shale gas production, and how the fracture permeability evolves remains poorly understood.

Previous experimental researches found that the fracture permeability may increase or decrease due to various mechanical, chemical, and thermal processes [35, 36]. The fracture permeability may increase through the free-face dissolution, while permeability decrease is observed through the processes such as clay mineral swelling, pressure solution, mechanical compaction, and secondary mineral precipitation [37–41]. Thus, a deep understanding of how fracture permeability evolves and the link between fracture permeability and microscale fracture surface alternation will help constrain the permeability evolution of shale fractures due to the Sc-CO_2 soak.

This study aims to understand how the shale fracture surface alters and how fracture permeability evolves after the Sc-CO_2 soak. We perform a series of fracture permeability measurements after the soak of shale fractures into Sc-CO_2 for 1, 3, 5, 7, and 14 days. Analysis techniques, including X-ray diffraction analysis (XRD), surface profilometry scanning, and nuclear magnetic resonance (NMR), are used to understand how the mineralogy, fracture surface roughness, and pore volume distribution change due to the Sc-CO_2 soak. Our results provide a deeper understanding of the alternation effect of Sc-CO_2 on the shale fracture permeability.

2. Samples and Experimental Method

The experimental study consists of several components: (a) shale samples soaking with Sc-CO_2 under the temperature of 50°C and 10 MPa for 1, 3, 5, 7, and 14 days; (b) shale fracture permeability measurement under the effective normal stress ranges from 1 to 20 MPa; (c) XRD tests for mineralogy analysis, NMR tests for shale pore characteristics analysis, and surface profilometry scanning tests for fracture surface roughness analysis.

2.1. Sample Preparation. The shale samples used in this research were collected from Lower Silurian Formation in Sichuan Basin, China, which was also the main shale gas producing area in China. The core samples were firstly drilled from the shale blocks with a diameter of 25.4 mm. Then, the shale samples were cut into a length of 50.8 mm. After that, the rock samples were saw-cut into two halves with a smooth fracture surface and later polished with the abrasive silicon carbide (20 grits, equivalent to 830 μm) to create rough fracture surfaces. The prepared shale samples are shown in Figure 1(a). Our previous research results indicated that this method creates fracture surfaces with similar fracture roughness to the fractures induced by Sc-CO_2 fracturing [16]. The mineralogical composition of shale samples is listed in Table 1. The main mineral is quartz, which accounts for 44.13% of total weight. Following that, illite accounts for 23.18% and 19.61% for calcite. Other minor minerals include dolomite and albite, which account for 8.59% and 4.49% separately. Furthermore, we group the minerals into three categories, tectosilicate, carbonate, and phyllosilicate, based on their structures [42].

2.2. Experiment Apparatus and Procedure. This research mainly involves two experimental apparatuses: (a) Sc-CO_2 soaking system and (b) permeability measurement apparatus. The Sc-CO_2 soaking system is shown in Figure 1(b), including a high-pressure vessel, constant temperature water bath, injection pump, and CO_2 cylinders. The high-pressure vessel has a capacity of 50.0 MPa. The water provides a constant temperature environment with an accuracy of ±0.05°C. The injection pump is an ISCO 260D syringe pump with a rate of 0.001 to 107 mL/min and the maximum fluid pressure at 51.7 MPa. Our experiment set the water bath temperature at 50°C and fluid pressure at 10.0 MPa, enabling the supercritical state of carbon dioxide. The soaking time was set to 1, 3, 5, 7, and 14 days.

After the Sc-CO_2 soaking of Longmaxi shale samples, we use the permeability measurement apparatus to measure the fracture permeability under various effective stress states, ranging from 1.0 to 20.0 MPa. The permeability measurement apparatus is shown in Figure 1(c). Pump A controls the

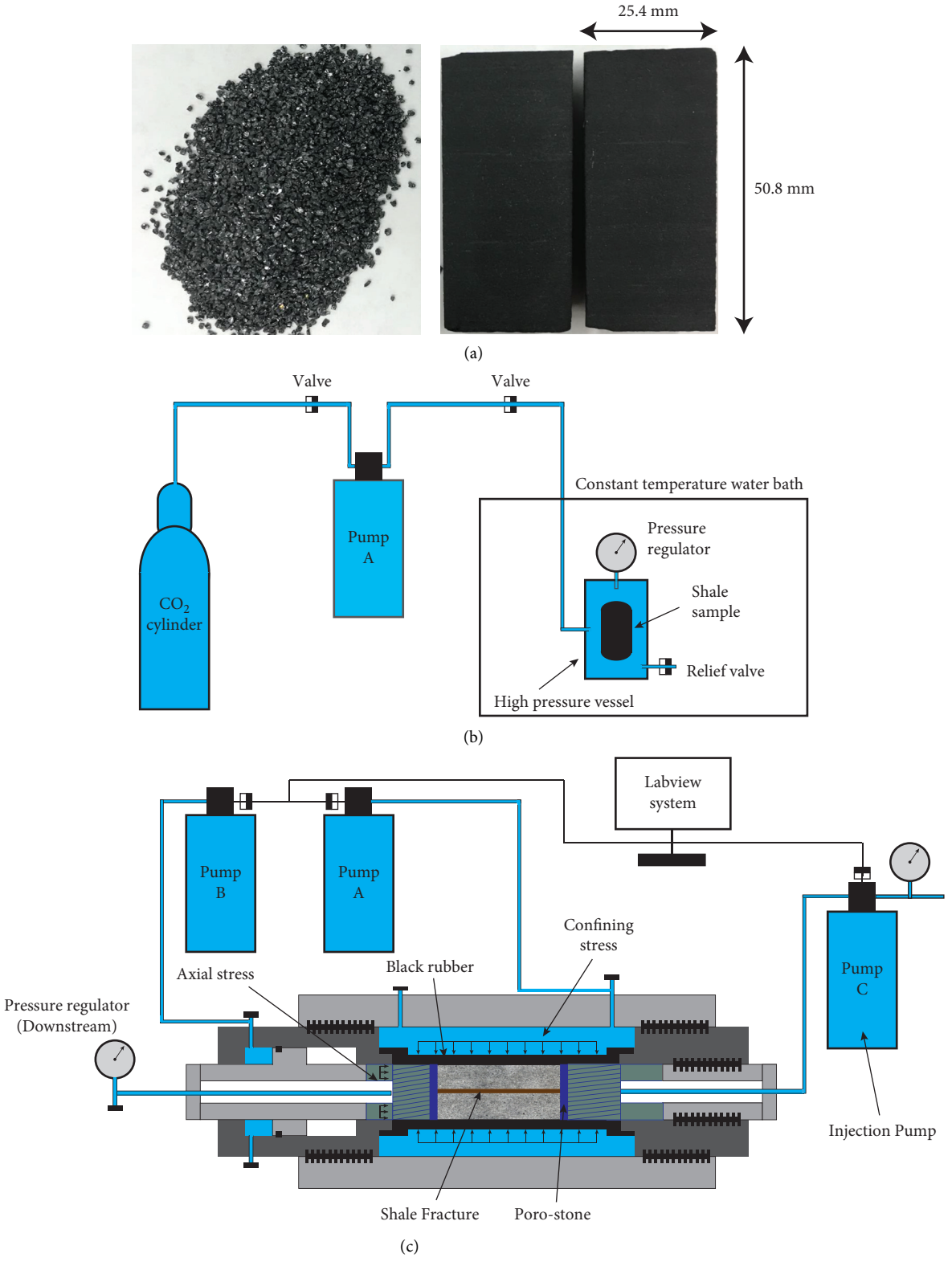

Figure 1: (a) The Longmaxi shale samples used for the tests. (b) The experimental apparatus for the CO_2 soak. (c) The permeability measurement apparatus.

confining stress of the shale fractures, and pump B controls the axial stress. Pump C controls a constant fluid pressure (200 kPa) in the upstream reservoir while the downstream reservoir is connected with the atmosphere. For our experiments, the Reynolds number could be estimated through the following equation:

Table 1: Detailed mineralogical compositions (wt%) of Longmaxi sample before experiments.

Mineral group	Mineral name	Weight percentage (%)	Total (%)
Tectosilicate	Quartz	44.13	48.62
	Albite	4.49	
Carbonate	Calcite	19.61	28.20
	Dolomite	8.59	
Phyllosilicate	Illite	23.18	23.18
Total		100	100

$$\mathrm{Re} = \frac{uL}{\nu} = \frac{\rho u L}{\mu}, \tag{1}$$

where ρ and μ are fluid density and dynamic viscosity, respectively. u is the flow speed and L is the characteristic linear dimension. Based on the experimental setup and experimental data, the fluid flow in the fractures is less than 1.0, and cubic law could be used to describe the linear Darcy flow [43]. Thus, the cubic law is used to calculate the fracture permeability and hydraulic aperture [44]:

$$e_f = -\frac{12 \times \mu_f \times L \times Q}{W \times \Delta P_f}, \qquad k = \frac{e_h^2}{12}, \tag{2}$$

where e_f is the fracture hydraulic aperture; k is the fracture permeability; μ_f is the dynamic viscosity of water; L is the contact length of the fracture; W is the width of the fracture; Q is the measured flow rate; ΔP_f is the fluid pressure difference between upstream and downstream reservoirs.

We used the powder of whole-rock fractions (<74.0 μm) for the XRD analysis. The Rigaku D/Max-2500 X-ray diffractometer was used to determine the mineralogical composition alternation due to the Sc-CO_2 soaking. The shale fracture samples were also characterised by the NMR analysis system, the MacroMR12-150H-I model. The NMR measured the pore size distribution of shale samples by detecting transverse (or spin-spin) relaxation time T_2. The detailed mechanism of pore size characterisation could be found in [45, 46]. Moreover, the SEM images provided a direct visualisation of pores, and the apparatus we used in this research was FEI Quanta 600. After the Sc-CO_2 soaking for various times, the fracture surface roughness was also characterised by a Zygo™ NewView optical profilometer [47]. The parameter, root mean square roughness, is used to represent the fracture roughness, which describes the profile height deviations from the mean line.

3. Experimental Results and Discussions

In this part, we present the permeability measurement results of shale fractures after soaking with Sc-CO_2 for 1, 3, 5, 7, and 14 days. Then, the XRD results are shown to indicate the mineralogical compositions evolution in shale fractures. After that, the sample porosity and pore volume alternation due to Sc-CO_2 soaking are shown. Finally, SEM images and fracture surface roughness are used to indicate how Sc-CO_2 soaking changes the fracture surface structure and topography characteristics.

3.1. Fracture Permeability Evolution due to Sc-CO_2 Soaking. The fracture permeability evolution results are shown in Figure 2(a). Since the fracture permeability is a stress-dependent parameter and the fracture permeability is measured under the effective stress of 1.0, 5.0, 10.0, 15.0, and 20.0 MPa. The fracture permeability decreases with the increase of the effective normal stress, which is the result of fracture closure. Under the effective normal stress of 1.0 MPa, the fracture permeability is 5.96×10^{-12} m^2 for fractures not treated with Sc-CO_2. With the soaking time ranges from 1, 3, 5, 7, and 14 days, the fracture permeability decreases to 1.07×10^{-11}, 1.64×10^{-11}, 2.47×10^{-11}, 3.84×10^{-11}, and 4.35×10^{-11} m^2. Thus, a 7.3 times increase of fracture permeability is observed after 14 days of Sc-CO_2 under the effective normal stress of 1.0 MPa. Similarly, under the effective normal stress of 20.0 MPa, the fracture permeability is 1.30×10^{-12} m^2 for untreated fractures. While with the soaking with Sc-CO_2, the fracture permeability increases to 3.54×10^{-12}, 5.95×10^{-12}, 8.67×10^{-12}, 1.38×10^{-11}, and 1.55×10^{-11} m^2 after 1, 3, 5, 7, and 14 days. Moreover, we use the cubic law to calculate the fracture aperture from the fracture permeability data and plot the results in Figure 2(b). Similar trends are observed since the fracture permeability and fracture aperture has the same physical meaning in this research. Under the effective normal stress of 1.0 MPa, the fracture aperture increases from 8.46 μm to 11.35, 14.05, 17.21, 21.45, and 22.85 μm after soaking with Sc-CO_2 for 1, 3, 5, 7, and 14 days. Under the effective normal stress of 20.0 MPa, fracture aperture increases from 3.95 μm to 6.52, 6.52, 8.45, 10.20, 12.85, and 13.65 μm after soaking with Sc-CO_2 for 1, 3, 5, 7, and 14 days. Thus, our experimental results indicate that the soaking with Sc-CO_2 will largely increase the shale fracture permeability and effective hydraulic aperture.

During the fracture permeability measurement, the normal stress applied on the fracture increases from 1.0 to 5.0, 10.0, and 15.0 and finally reaches 20.0 MPa. The permeability and effective hydraulic aperture decrease are the results of fracture closure. The parameter fracture normal stiffness is commonly used to characterise the fractures' ability to resist the normal closure, and the definition is the rate of change in normal stress with respect to fracture closure [48]:

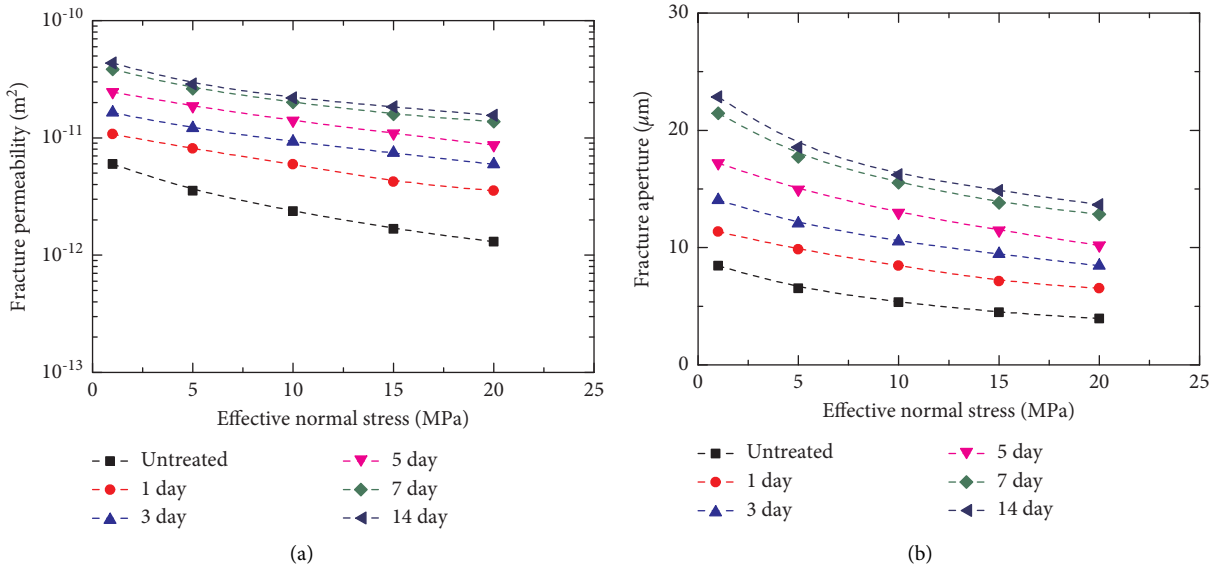

FIGURE 2: Permeability and hydraulic aperture evolution with effective normal stress for shale fractures after the Sc-CO_2 soak. (a) Fracture permeability and (b) fracture hydraulic aperture.

$$K_n = \frac{d\sigma_n}{du_n} = -\frac{d\sigma_n}{de_f}, \tag{3}$$

where u_n is the normal displacement (positive for closure), e_f is the fracture aperture, and σ_n is the effective normal stress applied on the fracture.

Thus, we plot the relationship between fracture normal closure and effective normal stress in Figure 3(a), and the results show a highly nonlinear normal closure behaviour of fractures due to the effective normal stress increase. In a recent model developed by Zangerl et al. [49], a linear relationship was proposed to constrain the relationship between the logarithm of effective normal stress and fracture normal closure:

$$\ln(\sigma_n) = A(-\Delta e_f) + B, \tag{4}$$

where A is a stiffness characteristic and B is the logarithm of the reference normal stress. Thus, we further plot the relationship between the logarithm of effective normal stress and fracture normal closure in Figure 3(b), where a linear relationship is presented.

Additionally, it could be found that fracture aperture is a stress-dependent parameter and the fracture stiffness is also largely affected by the effective normal stress. Thus, the relationship between normal stiffness and effective normal stress could be expressed as follows [50]:

$$k_n = \left(\frac{dk_n}{d\sigma_n}\right)\sigma_n. \tag{5}$$

where $dk_n/d\sigma_n$ is a constant that is referred to "stiffness characteristic" [49, 50]. Thus, we further plot the relationship between fracture normal stiffness and effective normal stress shown in Figure 3(c). A linear relationship is observed between fracture normal stiffness and effective normal stress. This observation is as same as laboratory-scale and in situ description of granite fractures.

The parameter-stiffness characteristic, $dk_n/d\sigma_n$, should be constant and independent with normal stress and could be used to describe the fracture's normal stiffness. Furthermore, we calculate the $dk_n/d\sigma_n$ evolution with soaking times for our fractures and plot this in Figure 3(d). The results show that the stiffness characteristics value decreases from 122.91 mm^{-1} to 73.57, 67.93, 69.17, 63.93, and 64.05 mm^{-1} after soaking with Sc-CO_2 for 1, 3, 5, 7, and 14 days. Thus, the fracture normal stiffness decreases with the increasing soaking times with Sc-CO_2, which indicates that the soaking with Sc-CO_2 will decrease normal stiffness. This observation is in accordance with the previous research that the exposure to the Sc-CO_2 will shale competencies and deteriorate its mechanical properties [31, 34]. Thus, the fractures will be more easily compressed and induce fracture aperture closure after soaking with Sc-CO_2. It is worth mentioning that the stiffness characteristics are 63.93 mm^{-1} and 64.05 mm^{-1} after soaking with Sc-CO_2 for seven days, separately. The similar values may indicate there may be a threshold for the fracture normal stiffness degradation: after seven days with Sc-CO_2 soaking, the fracture normal stiffness will reach a threshold value and will not decrease much for further soaking with Sc-CO_2.

3.2. Fracture Mineralogy Evolution due to Sc-CO_2 Soaking. To identify the possible chemical reactions that occur in the fracture surface due to Sc-CO_2 soaking and explore the mechanisms for fracture permeability evolution, we also performed the XRD analysis to quantify the mineralogical composition evolution [51]. As mentioned before, all minerals are grouped into three categories: tectosilicate, carbonate, and phyllosilicate, and we show three groups of mineralogy evolving with soaking times in Figure 4(a). The results show that the tectosilicate and phyllosilicate content increases slightly, while carbonate minerals content

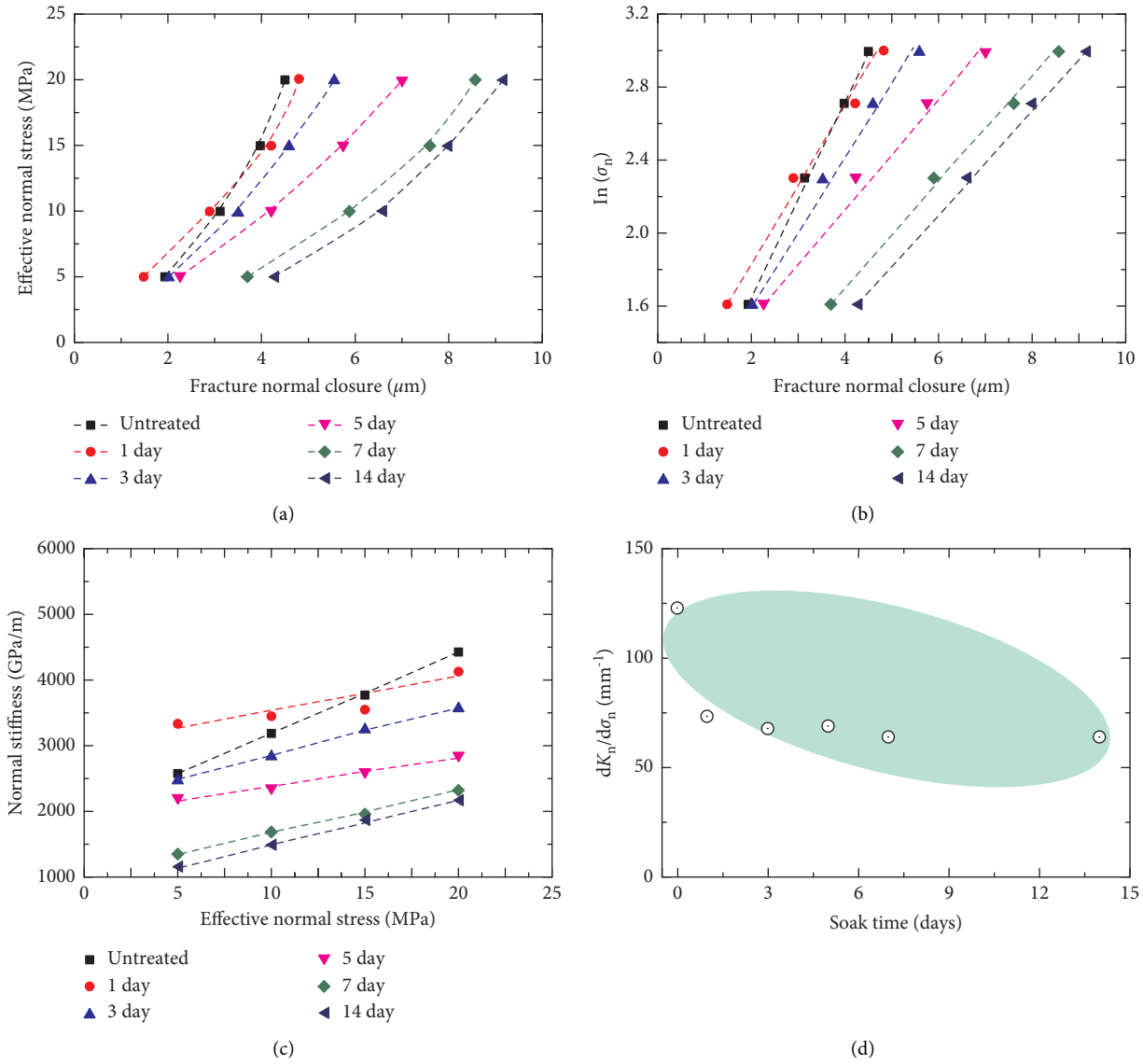

Figure 3: The logarithmic closure law describes the fracture closure. (a) The relationship between fracture normal closure and effective normal stress; (b) a linear relationship is observed for fracture normal closure and logarithmic normal stress; (c) the linear relationship between effective normal stress and fracture normal stiffness; (d) a decrease of stiffness characteristic value with soaking time.

decreases. Since the main carbonate minerals in Longmaxi shale are calcite and dolomite, we further plot the calcite and dolomite mineral evolution with soaking times in Figure 4(b). The results also indicate that both calcite and dolomite minerals contents decrease with soaking times. The alterations in mineralogical compositions should be related to the complicated chemical reaction between Sc-CO_2 and shale minerals. Previous researches have summarised some potential chemical reactions [26]:

$$\begin{aligned} &\text{calcite} + 2H^+ \leftrightarrow Ca^{2+} + CO_2 + H_2O, \\ &\text{dolomite} + 4H^+ \leftrightarrow Ca^{2+} + Mg^{2+} + 2CO_2 + 2H_2O. \end{aligned} \tag{6}$$

During the Sc-CO_2 soaking, H^+ may exist when CO_2 meets the original water in the shale samples, forming the carbonic acid (H_2CO_3). At the same time, calcite is a kind of stable polymorph of calcium carbonate ($CaCO_3$). Thus, the calcite may react with H^+ and result in the $Ca^{2+,}$ and through this process, the calcite mineral dissolves. Similarly, dolomite is composed of calcium magnesium carbonate, ideally, $CaMg(CO_3)_2$, and it may react with H^+ and result in Ca^{2+} and Mg^{2+}. Thus, the dissolution of calcite and dolomite will decrease the relative content with Sc-CO_2 soaking and induce the relative increase of the content of tectosilicate and phyllosilicate. It is also worth mentioning that after seven days of soaking, the mineral content does not change dramatically, which is in accordance with permeability evolution. Thus, we may believe seven days may be a threshold that the chemical reactions terminate, and the shale fractures become stable after seven days of soaking with Sc-CO_2.

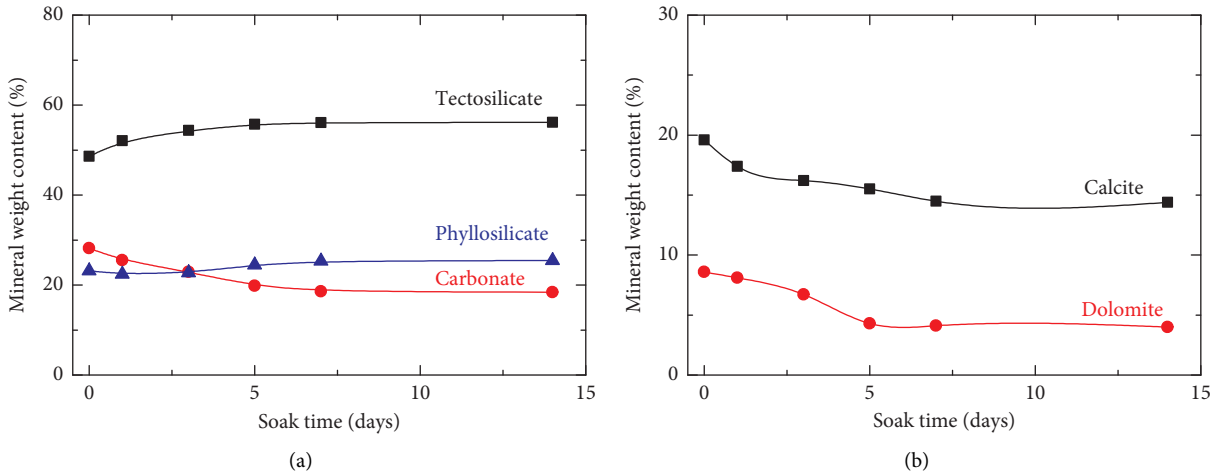

FIGURE 4: The mineralogical compositions evolution due to CO_2 soak. The tectosilicate minerals include quartz, analcime, anorthite, albite, and microcline. The carbonate minerals include carbonate and dolomite. The phyllosilicate minerals include muscovite, illite, chlorite, kaolinite, and montmorillonite. (a) The mineral weight content change due to the CO_2 soak. (b) The mineralogical content evolution of calcite and dolomite.

3.3. NMR Characterisation of Pore Volume Alternation. The NMR methods provide information on pore volume distribution of shale before and after Sc-CO_2 soaking. As shown in Figure 5, the pores could be divided into three categories: micropores with pore width less than 2 nm, mesopores with pore width between 2 and 50 nm, and macropores with a width larger than 50 nm. It could be easily observed that with the increase of soaking times, more pores with larger widths are observed. Additionally, we plot the pore width distribution under various soaking times in Figure 6(a). The mesopores are the dominant pore size for Longmaxi shale, with a content higher than 60%. With the increase of soaking times, the percentage of macropore increases from 26.89% for untreated samples to 27.11%, 29.05%, 30.21%, 32.15%, and 32.42% after soaking with Sc-CO_2 for 1, 3, 5, 7, and 14 days. Simultaneously, the percentage of mesopores and micropores has slightly decreased due to the increase of pore width, which means that the pore width distribution curves move rightwards. This observation is also in accordance with the results of average pore width, as shown in Figure 6(b). With the increase of soaking times, the average pore width increases from 11.05 nm for untreated samples to 12.35, 14.09, 15.88, 16.44, and 16.69 nm after soaking with Sc-CO_2 for 1, 3, 5, 7, and 14 days. The average pore width results also validate our previous observations that after seven days of soaking with Sc-CO_2, the chemical reactions terminate since the pore width after seven days of soaking has almost the same pore width as samples after 14 days of soaking.

3.4. SEM Analysis of Fracture Surfaces Evolution. We also present SEM images of fracture surfaces after soaking with Sc-CO_2 for various days. It should be mentioned that the fracture surfaces were scanned after soaking with Sc-CO_2 but before the fracture permeability tests. The SEM images are summarised in Figure 7. Those images were captured with the high voltage at 20 kV, and magnification was 1500

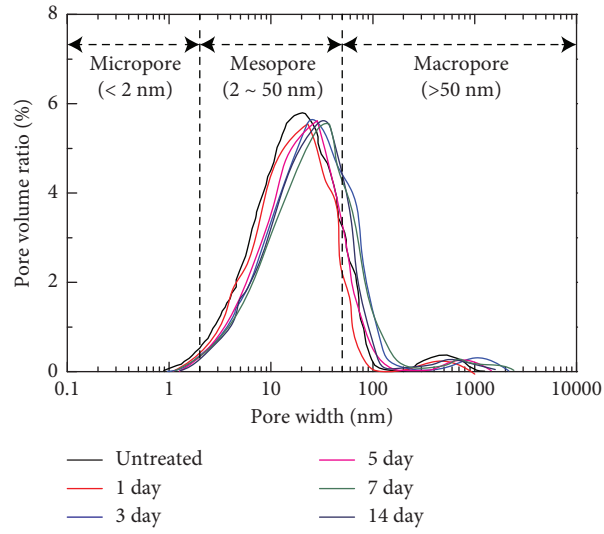

FIGURE 5: The pore widths evolution before and after CO_2 soak.

times. For untreated shale samples, we cannot see any large pores within the scope. After one day of soaking with Sc-CO_2, some large pores could be observed in the scope (marked with green boundary). Those pores may be the results of the dissolution of calcite and dolomite minerals. Additionally, with increasing soaking times, it is obvious that larger pores are shown in the scanning scopes. For the cases of soaking times at three and five days, it is interesting to see some undissolved minerals within the pores, which we mark with the red boundaries. Those minerals may need more time to be dissolved, and we cannot see those inner-pores minerals after soaking times more than seven days.

3.5. Fracture Surface Roughness Evolution. The optical profilometry method is used to quantify the shale fracture roughness evolution due to the soaking with Sc-CO_2 and

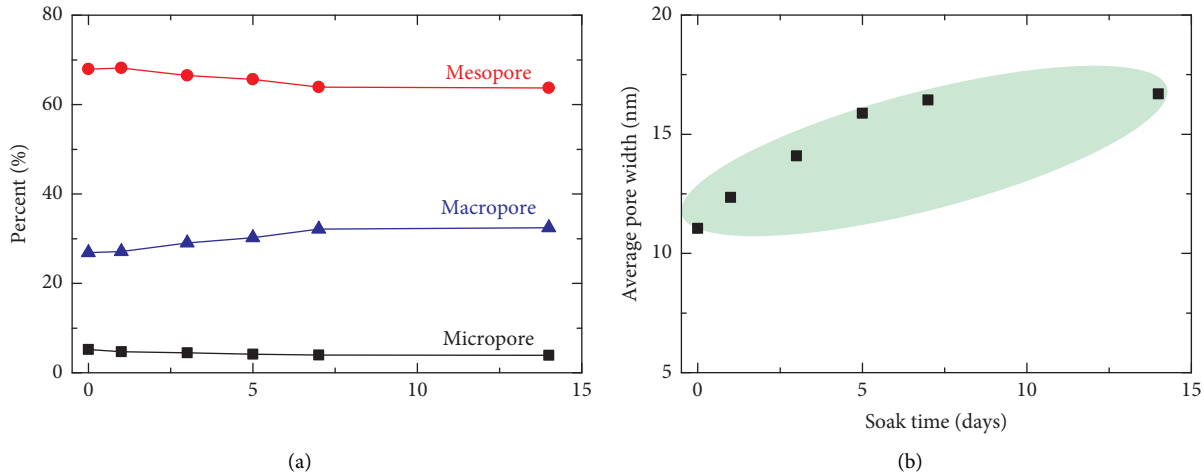

Figure 6: Pore volume and averaged pore volume alternation due to CO_2 soak.

compression effect during the permeability tests, as shown in Figure 8. The black squares and red circles in Figure 8 represent the root mean square roughness after the soaking and before the permeability tests. The results show that the root mean square roughness increases from 26.19 μm to 29.33, 33.14, 35.12, 39.14, and 40.12 μm after soaking with Sc-CO_2 for 1, 3, 5, 7, and 14 days. The fracture roughness should be the result of carbonate mineral dissolution, in which the calcite and dolomite minerals are dissolved and removed with water. The removed minerals leave pore spaces in the fracture surface and thus create more valleys and increase the root mean square roughness. While after the permeability measurement, the root mean square roughness decreases to 20.21, 23.22, 26.54, 28.33, 30.32, and 29.14 μm, as shown by the red circles in Figure 8. The roughness reduction is the result of mechanical reduction of fracture asperities during permeability measurement tests where the effective normal stress increases from 0 to a maximum of 20.0 MPa. The increase of effective normal stress compacts the fracture surface asperities and causes plastic deformation or damage that cannot be recovered. The reduction of root mean square roughness is also plotted in Figure 8 by the blue triangles. It is interesting to observe that a severe roughness reduction and possible fracture asperities damage are shown with the increase of soaking times. This observation is in accordance with our previous analysis of fracture stiffness characteristics. With the soaking of Sc-CO_2, the shale fractures are more easily damaged, and the decrease of normal stiffness is observed (Figure 3(d)).

4. Implications for Sc-CO_2 Fracturing and Potential CO_2 Sequestration

Our experimental observations indicate that the soaking with Sc-CO_2 increases the fracture permeability by ~7.3 times and the corresponding fracture aperture ~2.7 times after 14 days. The XRD and SEM results showed that shale fracture permeability increase results from calcite and dolomite mineral dissolution and more pore spaces are created in the fracture surfaces. Another critical issue is the time threshold for Sc-CO_2, and shale reaction may last for seven days. The shale fracture permeability will stay stable, and fracture surface roughness does not change much. Those observations may deepen our understanding of Sc-CO_2 as the fracturing fluid for shale gas hydraulic fracturing and potential CO_2 sequestration in shale reservoirs.

Sc-CO_2 fluid has been proposed as the fracturing fluid candidate for shale reservoir hydraulic fracturing operations due to its possibility of lowering the breakdown pressure and creating complex fracture networks [16, 19]. During the hydraulic fracturing operations, the fluid injection may last one to two weeks based on the reservoir volume. Based on the results in our research, after creating hydraulic fractures in shale reservoirs, the fracture permeability may increase several times due to the continuous Sc-CO_2 injection through the carbonate mineral dissolution process. However, fracturing-induced fractures are easily compressed due to the in situ stress since the depth may be larger than 5,000 m, and the effective normal stress may be larger than 100.0 MPa. The exposure of shale fractures to Sc-CO_2 will decrease the fracture stiffness, which may induce larger fracture closure under the in situ stress states. Thus, some last steps such as proppant injection should be performed to keep the fracture open and for effective shale gas production.

As for the deep geological CO_2 sequestration, the low permeability shale could be the target formation since it has high ability to absorb CO_2 in the shale matrix. One critical factor that determines whether CO_2 sequestration is a success is the long-term sealability of the reservoir. Thus, fractures and faults should be avoided in the sealing reservoirs. As we observed in this study, the shale fracture permeability may increase several times, and those fractures may work as the CO_2 leakage paths. On the one hand, those fractures and faults should be carefully understood before the large-scale injection of CO_2 into the reservoir through geological investigation. On the other hand, deep CO_2 sequestration is a long-timescale project, which aims to seal

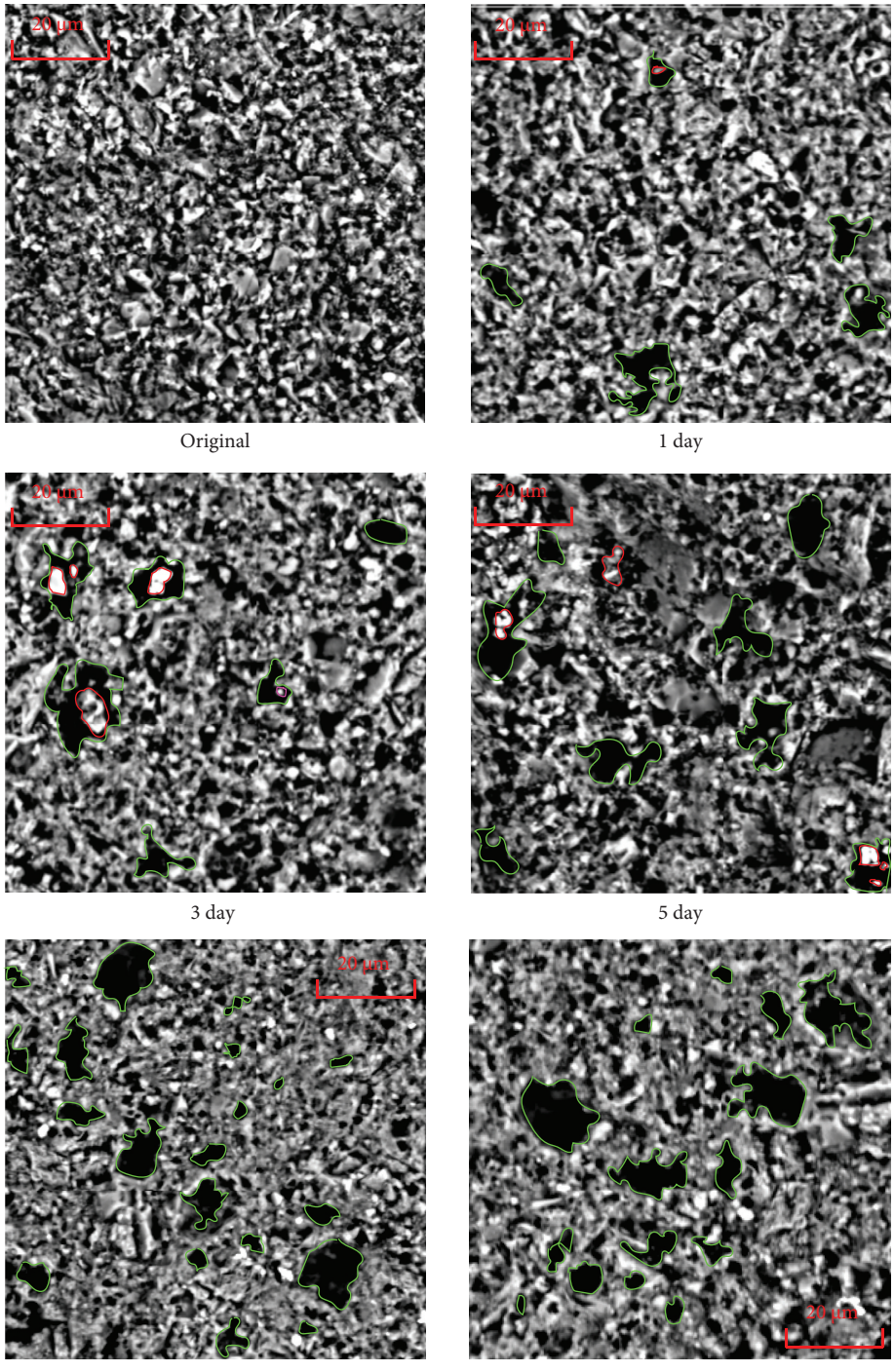

Figure 7: SEM images of shale fracture surfaces due to CO_2 soak. Green circles are pores that can be observed in the SEM images.

the CO_2 underground for hundreds and thousands of years. If the chemical reaction terminates after several days of soaking with CO_2 and the interactions between shale rock and CO_2 are weak after certain times, which is much less than the timescale of the whole project, the effect of CO_2 soaking on shale fracture permeability evolution may be neglected when considering the whole project design. Last but not least, geological CO_2 sequestration is a complicated process, and the original water content in the reservoir cannot be ignored, which may accelerate the chemical reactions between shale and Sc-CO_2, and further research is meaningful in this topic.

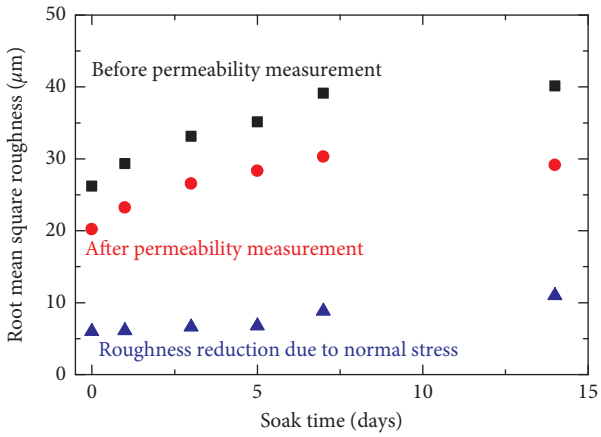

Figure 8: The fracture surface roughness (root mean square roughness) evolution before and after permeability measurement tests.

5. Concluding Remarks

We perform a series of shale fracture soaking tests with Sc-CO_2 and measure the fracture permeability evolution under various stress states to investigate the effect of Sc-CO_2 soaking on the shale fracture permeability evolution. Some supplementary test techniques are combined to identify the fracture mineralogical composition, pore characteristics, pore structure, and fracture roughness alternation from a microscale aspect. Our experimental observations indicate that the soaking with Sc-CO_2 may increase the shale fracture permeability through the chemical dissolution of calcite and dolomite minerals, which create more macropores in the fracture surface. The fracture aperture increase is in accordance with the observation of fracture surface roughness alternation, where peaks and valleys are formed. This chemical reaction process may last for almost seven days, after which the chemical interaction between shale fractures and Sc-CO_2 fluid may be neglected and the whole system becomes stable. Moreover, soaking with Sc-CO_2 will decrease the stiffness of shale fractures, which makes the fractures more easily compressed (close) due to effective normal stress. Our results validate the possibility that using Sc-CO_2 as the fracturing fluid may further increase the shale fracture permeability and reservoir permeability due to hydraulic fracturing. Due to its relatively short timescale, this process may not be that important in considering long-term deep CO_2 sequestration.

Data Availability

The data used to support the findings of this study are plotted within the article, and the raw data files are available by contacting the corresponding author.

Conflicts of Interest

The authors declared that there are no conflicts of interest regarding this work.

Acknowledgments

Zhaohui Lu acknowledges the funding from the National Natural Science Foundation of China (No. 52074059), Chongqing Science Foundation for Distinguished Young Scholars (cstc2021jcyj-jqX0007) and Performance Incentive Guidance Special Project of Chongqing Research Institutions (cstc2020jxjl90001). Pei He acknowledges the funding from the National Natural Science Foundation of China (No. 52004047). Yunzhong Jia acknowledges the support from the Open Project of National and Local Joint Engineering Research Center of Shale Gas Exploration and Development, Chongqing Institute of Geology and Mineral Resources (Project No. YYQGDZX-202002).

References

[1] X. Zhao and Y. Yang, "The current situation of shale gas in Sichuan, China," *Renewable and Sustainable Energy Reviews*, vol. 50, pp. 653–664, 2015.

[2] Y. Jia, Z. Lu, Q. Xiong, J. C. Hampton, Y. Zhang, and P. He, "Laboratory characterization of cyclic hydraulic fracturing for deep shale application in Southwest China," *International Journal of Rock Mechanics and Mining Sciences*, vol. 148, Article ID 104945, 2021.

[3] H. Nie, D. Li, G. Liu et al., "An overview of the geology and production of the Fuling shale gas field, Sichuan Basin, China," *Energy Geoscience*, vol. 1, no. 3-4, pp. 147–164, 2020.

[4] D. Rahm, "Regulating hydraulic fracturing in shale gas plays: the case of Texas," *Energy Policy*, vol. 39, no. 5, pp. 2974–2981, 2011.

[5] R. W. J. Edwards and M. A. Celia, "Shale gas well, hydraulic fracturing, and formation data to support modeling of gas and water flow in shale formations," *Water Resources Research*, vol. 54, no. 4, pp. 3196–3206, 2018.

[6] M. A. A. Ahamed, M. S. A. Perera, L. Dong-yin, P. G. Ranjith, and S. K. Matthai, "Proppant damage mechanisms in coal seam reservoirs during the hydraulic fracturing process: a review," *Fuel*, vol. 253, pp. 615–629, 2019.

[7] A. Vengosh, N. Warner, R. Jackson, and T. Darrah, "The effects of shale gas exploration and hydraulic fracturing on the quality of water resources in the United States," *Procedia Earth and Planetary Science*, vol. 7, pp. 863–866, 2013.

[8] J. D. Arthur, B. K. Bohm, B. J. Coughlin, M. A. Layne, and D. Cornue, "Evaluating the environmental implications of hydraulic fracturing in shale gas reservoirs," in *Proceedings of the SPE Americas E&P environmental and safety conference*, OnePetro, San Antonio, TX, USA, 2009 March.

[9] M. M. S. Yazdan, M. T. Ahad, I. Jahan, and M. Mazumder, "Review on the evaluation of the impacts of wastewater disposal in hydraulic fracturing industry in the United States," *Technologies*, vol. 8, no. 4, p. 67, 2020.

[10] R. Schultz, R. J. Skoumal, M. R. Brudzinski, D. Eaton, B. Baptie, and W. Ellsworth, "Hydraulic fracturing-induced seismicity," *Reviews of Geophysics*, vol. 58, no. 3, Article ID e2019RG000695, 2020.

[11] A. K. Quainoo, B. M. Negash, C. B. Bavoh, T. O. Ganat, and B. N. Tackie-Otoo, "A perspective on the potential application of bio-inhibitors for shale stabilization during drilling and hydraulic fracturing processes," *Journal of Natural Gas Science and Engineering*, vol. 79, Article ID 103380, 2020.

[12] P. Hou, F. Gao, Y. Ju et al., "Experimental investigation on the failure and acoustic emission characteristics of shale,

sandstone and coal under gas fracturing," *Journal of Natural Gas Science and Engineering*, vol. 35, pp. 211–223, 2016.

[13] T. Ishida, S. Desaki, Y. Kishimoto, M. Naoi, and H. Fujii, "Acoustic emission monitoring of hydraulic fracturing using carbon dioxide in a small-scale field experiment," *International Journal of Rock Mechanics and Mining Sciences*, vol. 141, Article ID 104712, 2021.

[14] I. Okamoto, X. Li, and T. Ohsumi, "Effect of supercritical CO_2 as the organic solvent on cap rock sealing performance for underground storage," *Inside Energy*, vol. 30, no. 11-12, pp. 2344–2351, 2005.

[15] T. Ishida, K. Aoyagi, T. Niwa et al., "Acoustic emission monitoring of hydraulic fracturing laboratory experiment with supercritical and liquid CO_2," *Geophysical Research Letters*, vol. 39, no. 16, 2012.

[16] Y. Jia, Y. Lu, D. Elsworth, Y. Fang, and J. Tang, "Surface characteristics and permeability enhancement of shale fractures due to water and supercritical carbon dioxide fracturing," *Journal of Petroleum Science and Engineering*, vol. 165, pp. 284–297, 2018.

[17] X. Zhang, Y. Lu, J. Tang, Z. Zhou, and Y. Liao, "Experimental study on fracture initiation and propagation in shale using supercritical carbon dioxide fracturing," *Fuel*, vol. 190, pp. 370–378, 2017.

[18] H. Chen, Y. Hu, Y. Kang, C. Cai, J. Liu, and Y. Liu, "Fracture initiation and propagation under different perforation orientation angles in supercritical CO2 fracturing," *Journal of Petroleum Science and Engineering*, vol. 183, Article ID 106403, 2019.

[19] Y. Jia, C. Song, J. Wang, and Q. Gan, "The breakdown process of low-permeable shale and high-permeable sandstone rocks due to non-aqueous fracturing: the role of fluid infiltration," *Journal of Natural Gas Science and Engineering*, vol. 89, Article ID 103873, 2021.

[20] H. Yin, J. Zhou, Y. Jiang, X. Xian, and Q. Liu, "Physical and structural changes in shale associated with supercritical CO2 exposure," *Fuel*, vol. 184, pp. 289–303, 2016.

[21] X. Luo, X. Ren, and S. Wang, "Supercritical CO2-water-shale interactions and their effects on element mobilization and shale pore structure during stimulation," *International Journal of Coal Geology*, vol. 202, pp. 109–127, 2019.

[22] Q. Lyu, X. Long, P. G. Ranjith, J. Tan, Y. Kang, and Z. Wang, "Experimental investigation on the mechanical properties of a low-clay shale with different adsorption times in sub-/supercritical CO2," *Inside Energy*, vol. 147, pp. 1288–1298, 2018.

[23] Y. Pan, D. Hui, P. Luo, Y. Zhang, L. Sun, and K. Wang, "Experimental investigation of the geochemical interactions between supercritical CO2 and shale: implications for CO2 storage in gas-bearing shale formations," *Energy and Fuels*, vol. 32, no. 2, pp. 1963–1978, 2018.

[24] G. Feng, Y. Kang, Z.-d. Sun, X.-c. Wang, and Y.-q. Hu, "Effects of supercritical CO2 adsorption on the mechanical characteristics and failure mechanisms of shale," *Inside Energy*, vol. 173, pp. 870–882, 2019.

[25] Q. Lyu, X. Long, R. Pg et al., "A laboratory study of geomechanical characteristics of black shales after sub-critical/super-critical CO2 + brine saturation," *Geomechanics and Geophysics for Geo-Energy and Geo-Resources*, vol. 4, no. 2, pp. 141–156, 2018.

[26] J. Zhou, K. Yang, S. Tian et al., "CO2-water-shale interaction induced shale microstructural alteration," *Fuel*, vol. 263, Article ID 116642, 2020.

[27] X. Ao, Y. Lu, J. Tang, Y. Chen, and H. Li, "Investigation on the physics structure and chemical properties of the shale treated by supercritical CO2," *Journal of CO2 Utilization*, vol. 20, pp. 274–281, 2017.

[28] R. Lahann, M. Mastalerz, J. A. Rupp, and A. Drobniak, "Influence of CO2 on new albany shale composition and pore structure," *International Journal of Coal Geology*, vol. 108, pp. 2–9, 2013.

[29] M. H. Bhuiyan, N. Agofack, K. M. Gawel, and P. R. Cerasi, "Micro- and macroscale consequences of interactions between CO2 and shale rocks," *Energies*, vol. 13, no. 5, p. 1167, 2020.

[30] Y. Jiang, Y. Luo, Y. Lu, C. Qin, and H. Liu, "Effects of supercritical CO2 treatment time, pressure, and temperature on microstructure of shale," *Inside Energy*, vol. 97, pp. 173–181, 2016.

[31] R. Rezaee, A. Saeedi, S. Iglauer, and B. Evans, "Shale alteration after exposure to supercritical CO2," *International Journal of Greenhouse Gas Control*, vol. 62, pp. 91–99, 2017.

[32] B. L. Alemu, P. Aagaard, I. A. Munz, and E. Skurtveit, "Caprock interaction with CO2: a laboratory study of reactivity of shale with supercritical CO2 and brine," *Applied Geochemistry*, vol. 26, no. 12, pp. 1975–1989, 2011.

[33] S. Sanguinito, A. Goodman, M. Tkach et al., "Quantifying dry supercritical CO2-induced changes of the Utica Shale," *Fuel*, vol. 226, pp. 54–64, 2018.

[34] A. Fatah, H. B. Mahmud, Z. Bennour, M. Hossain, and R. Gholami, "Effect of supercritical CO2 treatment on physical properties and functional groups of shales," *Fuel*, vol. 303, Article ID 121310, 2021.

[35] C. Noiriel, B. Madé, and P. Gouze, "Impact of coating development on the hydraulic and transport properties in argillaceous limestone fracture," *Water Resources Research*, vol. 43, no. 9, Article ID W09406, 2007.

[36] G. Izadi and D. Elsworth, "The influence of thermal-hydraulic-mechanical- and chemical effects on the evolution of permeability, seismicity and heat production in geothermal reservoirs," *Geothermics*, vol. 53, pp. 385–395, 2015.

[37] J. Taron and D. Elsworth, "Constraints on compaction rate and equilibrium in the pressure solution creep of quartz aggregates and fractures: controls of aqueous concentration," *Journal of Geophysical Research: Solid Earth*, vol. 115, no. B7, 2010.

[38] Y. Jia, Y. Fang, D. Elsworth, and W. Wu, "Slip velocity dependence of friction-permeability response of shale fractures," *Rock Mechanics and Rock Engineering*, vol. 53, pp. 1–13, 2019.

[39] P. Szymczak and A. J. C. Ladd, "Microscopic simulations of fracture dissolution," *Geophysical Research Letters*, vol. 31, no. 23, 2004.

[40] H. Kumar, D. Elsworth, J. P. Mathews, and C. Marone, "Permeability evolution in sorbing media: analogies between organic-rich shale and coal," *Geofluids*, vol. 16, no. 1, pp. 43–55, 2016.

[41] H. Yasuhara, D. Elsworth, and A. Polak, "Evolution of permeability in a natural fracture: significant role of pressure solution," *Journal of Geophysical Research: Solid Earth*, vol. 109, no. B3, 2004.

[42] M. An, F. Zhang, D. Elsworth, Z. Xu, Z. Chen, and L. Zhang, "Friction of Longmaxi shale gouges and implications for seismicity during hydraulic fracturing," *Journal of Geophysical Research: Solid Earth*, vol. 125, no. 8, Article ID e2020JB019885, 2020.

[43] P. G. Ranjith and D. R. Viete, "Applicability of the 'cubic law' for non-Darcian fracture flow," *Journal of Petroleum Science and Engineering*, vol. 78, no. 2, pp. 321–327, 2011.

[44] R. W. Zimmerman and G. S. Bodvarsson, "Hydraulic conductivity of rock fractures," *Transport in Porous media*, vol. 23, no. 1, pp. 1–30, 1996.

[45] P. B. Basan, B. D. Lowden, P. R. Whattler, and J. J. Attard, "Pore-size data in petrophysics: a perspective on the measurement of pore geometry," *Geological Society, London, Special Publications*, vol. 122, no. 1, pp. 47–67, 1997.

[46] Y. Liu, Y. Yao, D. Liu, S. Zheng, G. Sun, and Y. Chang, "Shale pore size classification: an NMR fluid typing method," *Marine and Petroleum Geology*, vol. 96, pp. 591–601, 2018.

[47] Z. Song, Y. Wang, H. Konietzky, and X. Cai, "Mechanical behavior of marble exposed to freeze-thaw-fatigue loading," *International Journal of Rock Mechanics and Mining Sciences*, vol. 138, Article ID 104648, 2021.

[48] X.-W. Jiang, L. Wan, X.-S. Wang, S.-H. Liang, and B. X. Hu, "Estimation of fracture normal stiffness using a transmissivity-depth correlation," *International Journal of Rock Mechanics and Mining Sciences*, vol. 46, no. 1, pp. 51–58, 2009.

[49] C. Zangerl, K. F. Evans, E. Eberhardt, and S. Loew, "Normal stiffness of fractures in granitic rock: a compilation of laboratory and in-situ experiments," *International Journal of Rock Mechanics and Mining Sciences*, vol. 45, no. 8, pp. 1500–1507, 2008.

[50] K. F. Evans, T. Kohl, L. Rybach, and R. J. Hopkirk, "The effects of fracture normal compliance on the long term circulation behavior of a hot dry rock reservoir: a parameter study using the new fully-coupled code'Fracture," in *Proceedings of the Geothermal Resources Council*, vol. 16, pp. 449–456, Davis, CA, USA, January 1992.

[51] Z. Song, T. Frühwirt, and H. Konietzky, "Inhomogeneous mechanical behaviour of concrete subjected to monotonic and cyclic loading," *International Journal of Fatigue*, vol. 132, Article ID 105383, 2020.